

Supporting Information

The thermal properties of the aqueous ZnO precursors were analyzed by differential scanning calorimetry (DSC), as shown in Figure S1. In the ZnO sample, two endothermic reaction peaks were found at 65 °C and 170 °C. The small endothermic peak at 45 °C could be attributed to the removal of excess ammonium hydroxide from the sample. No peaks were observed in the region between 170 °C and 220 °C. This suggests a complete conversion from ammine-hydroxo precursor to solid ZnO thin film at a temperature lower than 200 °C.

The chemical compositions of ZnO thin films were characterized by XPS. Figure S2 shows the O 1s spectrum of ZnO samples annealed at different temperatures. The O 1s peak could in each case be deconvoluted into three subpeaks at 530.0 ± 0.1 eV, 531.5 ± 0.1 eV, and 532.7 ± 0.1 eV. The subpeak at 530.0 ± 0.1 eV has the highest intensity. This subpeak can be attributed to the M-O-M lattice.¹ A higher M-O-M lattice subpeak intensity in Figure S2 suggests a more complete transformation from aqueous precursors to solid ZnO films. Subpeaks at 531.5 ± 0.1 eV and 532.7 ± 0.1 eV are related to metal hydroxide (M-OH) components and adsorbed oxygen components.²

Figure S3 shows a scanning electron microscopy (SEM) image of ZnO thin film spin-coated on ITO glass substrate. A dense and homogeneous ZnO surface with well-connected grains as shown in the image is critical for achieving high electron mobility in ZnO thin films and good performance in ZnO FETs.

According to SEM images shown in Figure S4, combustion-processed SA films exhibited dense and uniform surfaces. A dense and homogeneous film is required to reduce leakage current through the dielectric film.

The surface morphology of combustion-processed SA thin films was analyzed by atomic force microscopy (AFM), as shown in Figure S5. The root-mean-square roughness self-combustion precursor processed SA decreased from 0.46 nm to 0.20 nm as the amount of GPTMS was increased from 10 at% to 50 at%. A smaller roughness, 0.17 nm, was obtained in an SA film prepared with urea-based combustion precursor.

The frequency dependence of the capacitance of SA MIM capacitors prepared with both urea-based combustion precursor and self-combustion precursor is shown in Figure S6. For both types of SA MIM capacitors, capacitance decreases with the increase of frequency, leveling at a capacitance similar to that of pure aluminum oxide (without sodium ion-incorporation) in the high frequency region. The high capacitance observed at low frequency could be attributed to electric double layer formation caused by the polarization of alkali metal ions. This capacitance behavior is similar to that of a SA MIM capacitor fabricated at 500 °C with a conventional SA precursor.³ As shown in Figure S6 (b), the increased amount of GPTMS in SA led to a modest decrease in SA dielectric capacitance. However, polymerization of GPTMS and cross-linking with aluminum oxide did not greatly affect the polarization of sodium ions in aluminum oxide matrix as a high capacitance is observed in the low frequency region.

Additional breakdown voltage data for capacitors is shown in Figure S7.

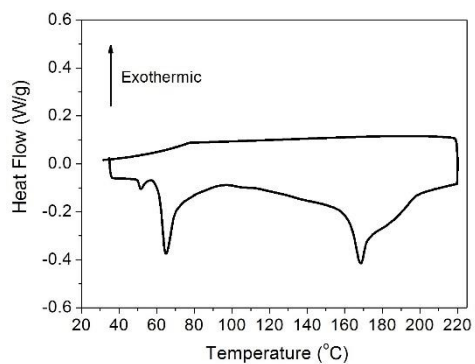


Figure S1. DSC scan of aqueous ZnO precursor.

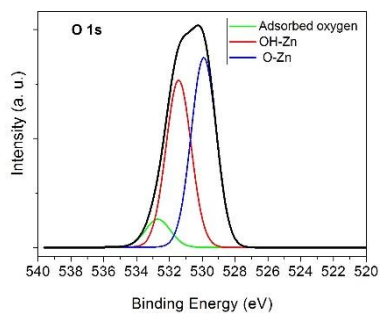


Figure S2. O 1s XPS spectrum of ZnO annealed at 200 °C for 1 hour.

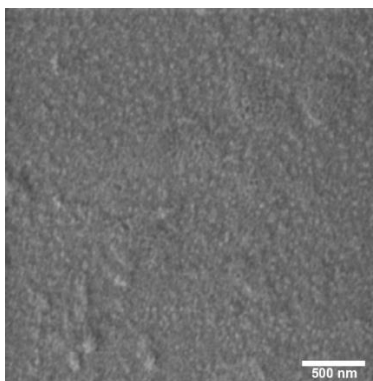


Figure S3. SEM image of ZnO annealed at 200 °C for 1 hour.

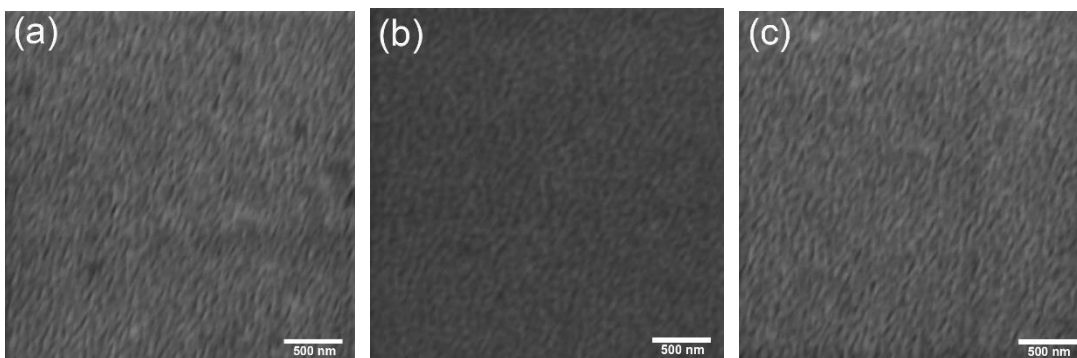


Figure S4. SEM image of SA thin film prepared by (a) urea based combustion precursor; (b) self-combustion precursor with 10 at% GPTMS; (c) self-combustion precursor with 50 at% GPTMS.

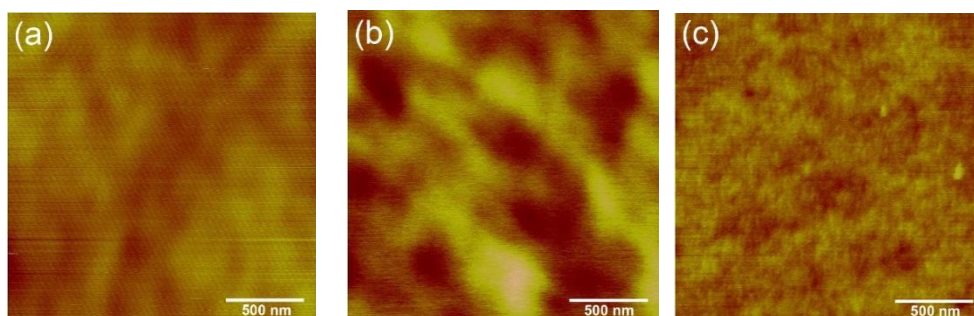
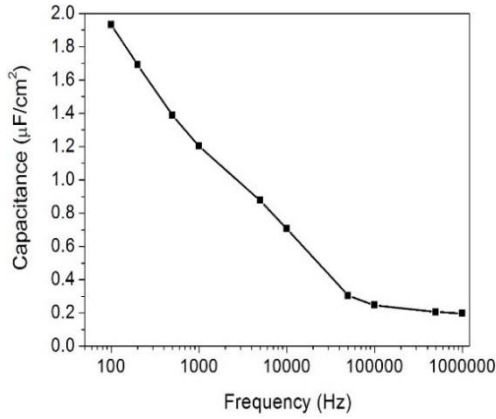
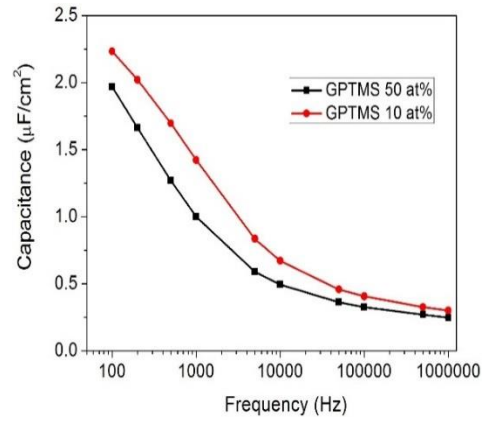


Figure S5. AFM image of SA film prepared by (a) urea-based combustion precursor; (b) self-combustion precursor with 10 at% GPTMS; (c) self-combustion precursor with 50 at% GPTMS.



(a)

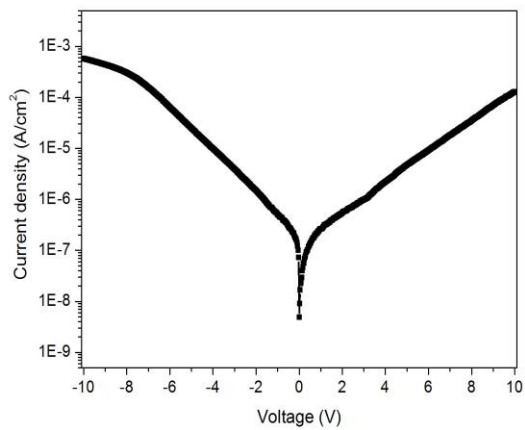


(b)

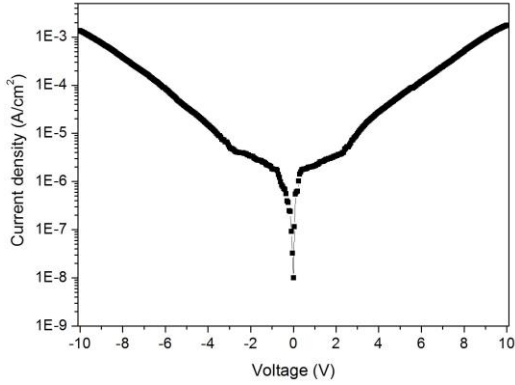
Figure S6. Frequency dependence of capacitance of (a) urea based combustion precursor prepared SA MIM capacitor and (b) self-combustion precursor prepared SA MIM capacitors with 10 at% and 50 at% GPTMS from 100 Hz to 1 MHz.

Figure S7 (below).

(a) Leakage current of SA dielectric film prepared by urea based precursor:



(b) Leakage current of SA dielectric film prepared by precursor with 10 at% GPTMS:



(c) Leakage current of SA dielectric film prepared by precursor with 50 at% GPTMS:

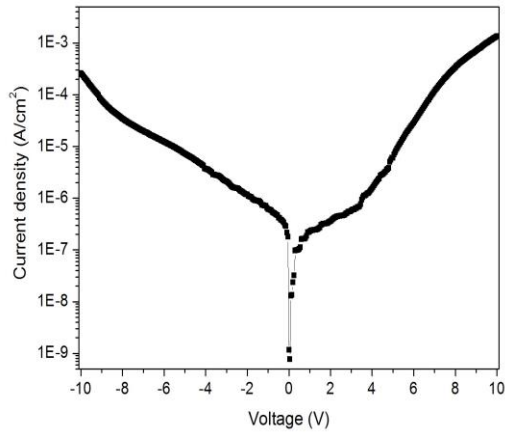


Table 1. Parameters for ZnO Devices.

Sample	No. of samples	Max. μ_{sat} ($\text{cm}^2 \cdot \text{V}^{-1} \cdot \text{s}^{-1}$)	Avg. μ_{sat} ($\text{cm}^2 \cdot \text{V}^{-1} \cdot \text{s}^{-1}$)	μ_{sat} Std.Dev. ($\text{cm}^2 \cdot \text{V}^{-1} \cdot \text{s}^{-1}$)	V_{th} (V) (Std.Dev.)	S (V/decade) (Std. Dev.)
ZnO based FETs with 300 nm SiO ₂ (Fig. 2)	30	0.7	0.5	0.26	5 (3.5)	5.2 (0.71)
ZnO on self-combustion processed SA isolated (Fig. 7)	5	1	0.5	0.37	1.4 (0.54)	0.54 (0.16)

References:

1. Donley, C.; Dunphy, D.; Paine, D.; Carter, C.; Nebesny, K.; Lee, P.; Alloway, D.; Armstrong, N. R. Characterization of Indium–Tin Oxide Interfaces Using X-ray Photoelectron Spectroscopy and Redox Processes of a Chemisorbed Probe Molecule: Effect of Surface Pretreatment Conditions. *Langmuir* **2002**, *18*, 450-457.
2. Hennek, J. W.; Smith, J.; Yan, A. M.; Kim, M. G.; Zhao, W.; Dravid, V. P.; Facchetti, A.; Marks, T. J. Oxygen “Getter” Effects on Microstructure and Carrier Transport in Low Temperature Combustion-Processed a-InXZnO (X = Ga, Sc, Y, La) Transistors. *J. Am. Chem. Soc.* **2013**, *135*, 10729-10741.
3. Liu, Y.; Guan, P.; Zhang, B.; Falk, M. L.; Katz, H. E. Ion Dependence of Gate Dielectric Behavior of Alkali Metal Ion-Incorporated Aluminas in Oxide Field-Effect Transistors. *Chem. Mater.* **2013**, *25*, 3788-3796.

